Jurnal Tribologi 16 (2018) 1-14

MYTRIBOS Malaysian Tribology Society

Jurnal Tribologi

Website : jurnaltribologi.mytribos.org e-issn: 2289-7232

Transient response of two lobe aerodynamic journal bearing

Saurabh Kumar Yadav [1,*], Nathi Ram [2]

[1] Department of Mechanical Engineering, Institute of Infrastructure Technology Research and Management, Ahmedabad, INDIA.
[2] Department of Mechanical & Automation Engineering, Indira Gandhi Delhi Technical University for Women, Kashmere Gate, Delhi-110006, INDIA.
[*]Corresponding author: saurabhme.iitr@gmail.com

KEYWORDS

Bifurcation diagram
Aerodynamic journal bearing
Transient response

ABSTRACT

The dynamic behavior of a rotor-dynamic system is greatly affected by the performance of aerodynamic bearing and the performance of bearing is characterized by the stiffness and damping coefficients. In the present work, stiffness and damping coefficients of bearing are computed and the performance of the bearing is greatly changed with the change in bearing air film profile. The effect of lobe offset factors on the transient performance of aerodynamic bearing is presented. Bifurcation and Poincare diagrams of two lobe journal bearing have been presented for different offset factors. A bearing designer can judge the bearing performance based on bifurcation diagrams.

Nomenclature

A	Area, (m^2)
$C_{x,y}$	Air film damping coefficient, (Ns/m)
D	Diameter of Rotor diameter
F_g	Resultant air film reaction force, $\sqrt{F_{gx}^2 + F_{gy}^2}$
F_e	External force, (N)
h	Local air film thickness, (m)
c	Radial clearance in horizontal direction when rotor is in centre
c_m	Radial clearance in vertical direction, (m)
p	Air film pressure, (N/m^2)
p_s, p_a	Ambient pressure, (N/m^2)
Q	Bearing flow, (m^3/s)

Received 30 June 2017; received in revised form 04 Sept 2017; accepted 10 Dec 2017.
To cite this article: Saurabh and Nathi (2018). Transient response of two lobe aerodynamic journal bearing. Jurnal Tribologi 16, pp.1-14.

n	Total number of nodes
n_t	Total number of elements
$S_{x,z}$	Air film stiffness coefficient, (N/m)
R	Radius of journal/rotor, (m)
M_j	Mass of the journal/rotor, (kg)
x_j, z_j	Coordinates of journal/rotor centre
t	Time, (s)
δ	Offset ratio, $\frac{c_m}{c}$
μ	Viscosity of the air, (Pa.s)
ρ	Density of the air, (kg/m^3)
ρ_c	Density of the air in cavitation region, (kg/m^3)
λ	Aspect ratio, $\lambda = L/D$
X, Y, Z	Cartesian coordinate system

Non-dimensional parameters

$\bar{C}_{x,z}$	$C_{x,z} \times \frac{c\omega}{R^2 p_s}$
$\bar{F}_g$	$\frac{F_g}{R^2 p_s}$
$\bar{F}_{rx}$	$\frac{F_{rx}}{R^2 p_s}$
$\bar{F}_{rz}$	$\frac{F_{rz}}{R^2 p_s}$
h	$\frac{h}{c}$
$X_j, \bar{x}_j$	$\frac{x_j}{c}$
$Z_j, \bar{z}_j$	$\frac{z_j}{c}$
$\dot{\bar{h}}$	$\frac{\partial \bar{h}}{\partial \tau}$
$V_x, \dot{\bar{x}}_j$	$\frac{\partial \bar{x}_j}{\partial \tau}$
$V_z, \dot{\bar{z}}_j$	$\frac{\partial \bar{z}_j}{\partial \tau}$
$\bar{p}$	$\frac{p}{p_s}$
$\bar{Q}$	$\frac{\mu}{p_s h_r^3} Q$
$\bar{M}_j$	$M_j \times \frac{mc\omega^2}{p_a R^2}$
$\bar{S}_{x,z}$	$S_{x,z} \times \frac{c}{R^2 p_s}$
$\bar{\omega}$	$\frac{R^2 \mu \omega}{p_s \times c^2}$
α	$\frac{X}{R}$
β	$\frac{Y}{R}$
τ	$t\omega$
$\bar{\mu}$	$\frac{\mu}{\mu_r}$

Subscripts and superscripts

b	Bearing
e	e^{th} element
0	Steady state equilibrium
N	Time interval level
–	Corresponding dimensionless parameter
s	Supply pressure

Matrices

$[\boldsymbol{F_1}], [\boldsymbol{F_2}], [\boldsymbol{F_3}], [\boldsymbol{F_4}]$	Assembled air fluidity Matrix
$\{\overline{\mathbf{p}}\}$	Nodal pressure Vector
$\{\overline{\mathbf{Q}}\}$	Nodal Flow Vector
$\{\overline{\boldsymbol{R}}_{\boldsymbol{Hi}}\}$	Right hand side column vector due to velocity
$\{\overline{\boldsymbol{R}}_{\boldsymbol{x,z}}\}$	Right hand side vector due to squeeze terms

1.0 INTRODUCTION

Air film journal bearings are used in navigational gyros, cryogenic engines, expansion turbine, air cycle machines and precision equipment. These bearings have certain favourable characteristics such as low friction, high value of air film stiffness and damping coefficient (Elrod et al., 1967; Yabe and Ikuno 1996; Lihua et al., 2007; Yang et al., 2014). Due to this, over the past decades of years, it has been an area of investigation by many researchers. They highlighted the static and dynamic response of air lubricated journal bearings. (Yang et al., 2014) presented a new nonlinear dynamic analysis method of rotor system supported by oil-film journal bearing. They extended the partial derivative method to second order approximate to predict the non-linear dynamic oil film stiffness and damping coefficient. They computed nonlinear dynamic performance of a symmetrical flexible rotor-bearing system via the journal orbit and Poincaré map. They show that the non-linear oil film forces by dynamic coefficients has universal applicability and help in the nonlinear dynamic analysis of rotor systems. (Chen and Yau 1998) studied the chaos in the flexible rotor supported by oil film bearing by using fractal dimension concept. They found that the dimension of the bearing centre trajectory is fractal and greater than two in some operating conditions. They suggested that a number of existing life-critical fluid film bearing systems are possible operated in chaotic region and fluid film system should be evaluated in terms on their mathematical observation. (Piekos, 2000) simulated the gas lubricated journal bearings for microfabricated machines by using orbit formulation method. They developed two numerical tools for orbit formulation. First was BASICS and second was SPECTURE. BASICS was written to examine effects invisible to tools constructed via the standard assumptions of lubrication theory. SPECTRES provided steady-state and stability data for the high eccentricities required by microbearings that was impossible with the low-order Galerkin methods and impractical with finite difference methods.

The nonlinear response of bearing is essential to predict the precise value of bearing stability. Therefore, various attempts have been made by researchers to accurately compute the exact response of dynamic behaviour of bearing. For the increasing value of mass, a chaotic behavior has been observed in the rotor motions. In the present work, Bifurcation diagram has been plotted by computing stiffness and damping coefficients. Bifurcation diagram is used to judge the performance of two lobe aerostatic journal bearing. It is found that two lobe bearing provided

better stability as compared to circular aerodynamic bearing. The results have been presented by using bifurcation diagrams and Poincaré maps. It is expected that results of present study will be quite useful for the bearing designer and academia community.

2.0 ANALYSIS

A schematic of air journal bearing has been shown in Figure 1. The non-dimensional governing Reynolds equation for air lubricated journal bearing is expressed as follows (Yadav et al., 2017; Malik and Bert 1994; Yang et al., 2009; Garg, 2015).

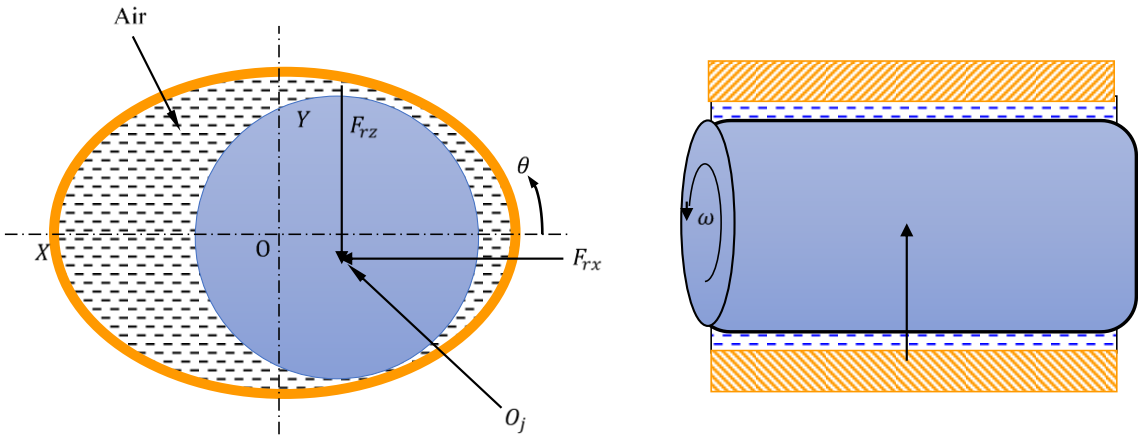

Figure 1(a): Schematic diagram of aerodynamic two lobe journal bearing.

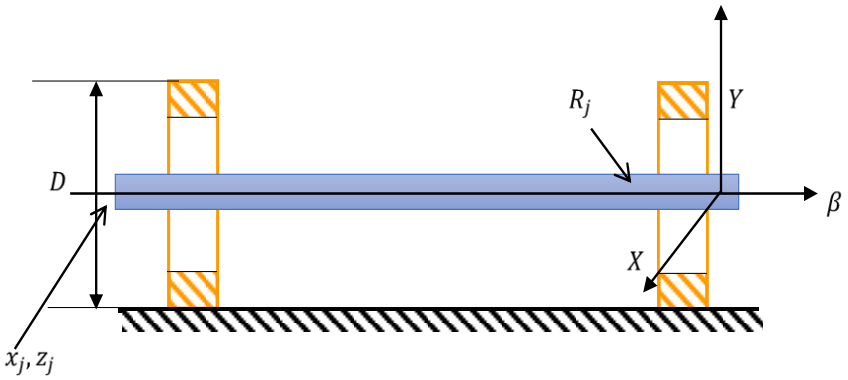

Figure 1(b): Schematic diagram of aerodynamic two lobe journal bearing.

$$\frac{\partial}{\partial\alpha}\left(\frac{\bar{h}^3}{12}\bar{p}\frac{\partial\bar{p}}{\partial\alpha}\right)+\frac{\partial}{\partial\beta}\left(\frac{\bar{h}^3}{12}\bar{p}\frac{\partial\bar{p}}{\partial\beta}\right)=\frac{\bar{u}}{2}\frac{\partial(\bar{p}\bar{h})}{\partial\alpha}+\frac{\partial(\bar{p}\bar{h})}{\partial\tau} \quad (1)$$

where, non-dimensional parameter $\bar{p} = \frac{p}{p_s}, \bar{h} = \frac{h}{C_r}, \bar{u} = \frac{R\omega}{P_a}\left(\frac{R}{C}\right)^2, \alpha = \frac{x}{R}, \beta = \frac{y}{R}, \tau = \omega t$

The fluid film thickness of two lobe aerodynamic journal bearing is computed by following expression (Kushare and Sharma 2014).

$$\bar{h} = 1 - (\bar{x}_j - \bar{x}_l)\sin(\theta) - (\bar{z}_j - \bar{z}_l)\cos(\theta) + \left(1 - \frac{1}{\delta}\right)\cos(\theta - \theta_l^k) \quad (2)$$

Where $\bar{x}_l, \bar{z}_l$ is the coordinates of lobe centre and θ_l^k is the lobe angle.
Where, $\frac{\partial \bar{h}}{\partial \tau} = -\bar{\dot{x}}_j \sin(\theta) - \bar{\dot{z}}_j \cos(\theta)$

3.0 FINITE ELEMENT FORMULATION

Finite element method is used to compute all the performance parameters because the solution of finite element method is more numerically stable than other methods, as shown in Figure 2.

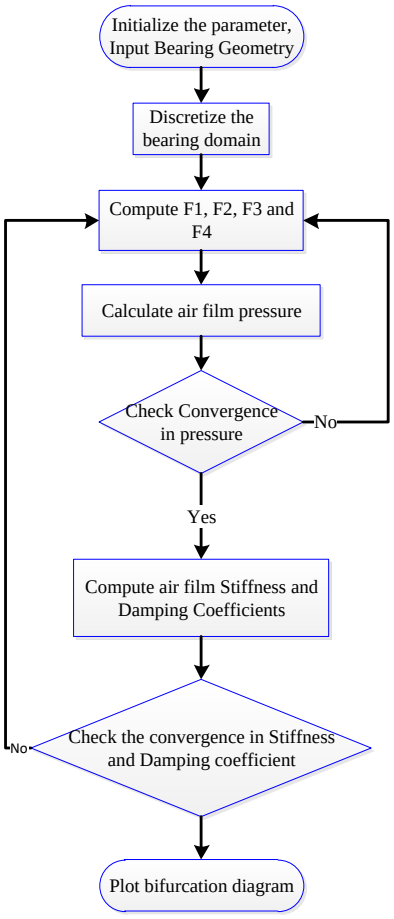

Figure 2: Solution flow scheme.

The air pressure variation over an element is computed as (Holster and Jacobs, 1987; Dhatt et al., 2012; Yadav and Sharma, 2014).

$$\bar{p} = \sum_{j=1}^{n_l^e} \bar{p}_j N_j \tag{3}$$

Where, N_j is the nodal shape function and n_l^e is number of nodes in a quadrilateral element. Here, the value of n_l^e is four. By applying Galerkin's orthogonality conditions and after the usual assembly procedure, the global system algebraic equation is expressed as follows (Sinhasan and Sah, 1996; Sharma et al., 2002).

$$[\overline{\boldsymbol{F}}]\{\overline{\boldsymbol{p}}\} = \{\overline{\boldsymbol{Q}}_{\boldsymbol{i}}\} + \boldsymbol{\omega}\{\boldsymbol{R_{Hi}}\} + \bar{\dot{\boldsymbol{x}}}_{\boldsymbol{j}}\{\overline{\boldsymbol{R}}_{\boldsymbol{x}}\} + \bar{\dot{\boldsymbol{z}}}_{\boldsymbol{j}}\{\overline{\boldsymbol{R}}_{\boldsymbol{z}}\} \tag{4}$$

The e^{th} element in the matrices are expressed as(Ma et al., 2016)

$$F_{ij}^e = \int\int \frac{h^3}{12}\bar{p}\left[\frac{\partial N_i}{\partial \alpha}\frac{\partial N_j}{\partial \beta} + \frac{\partial N_i}{\partial \alpha}\frac{\partial N_j}{\partial \beta}\right]\partial\Omega \tag{5a}$$

$$\bar{Q}_i^e = \oint\left\{\bar{p}\left(\bar{h}^3\frac{\partial \bar{p}}{\partial \alpha}\right)l_1 + \bar{p}\left(\frac{\partial \bar{h}}{\partial \alpha}\right)l_1 + \bar{p}\left(\bar{h}^3\frac{\partial \bar{p}}{\partial \beta}\right)l_2\right\}N_i d\Gamma^e \tag{5b}$$

$$\bar{R}_x^e = \int \bar{p}\cos(\alpha)N_i\partial\Omega \tag{5c}$$

$$\bar{R}_z^e = \int \bar{p}\sin(\alpha)N_i\partial\Omega \tag{5d}$$

Where l_1 and l_2 are directional vectors and *i*, *j*=1, 2 … n_l^e (number of nodes per element). Γ^e Is used for element boundary and e^{th} is the element number. The equation for global systems are obtained by assembling the elemental equations as per the connectivity of the element in domain (Awasthi et al. 2006).

4.0 BEARING PERFORMANCE PARAMETER

The computation of bearing statics and dynamic performance characteristics parameters (PCP) of an air bearing is quite involved as it requires lot of computation. The performance characteristics parameters of an aerodynamic bearing system is computed as follows.

4.1 Load carrying capacity

Fluid-film reaction components in x and z directions are computed by using the following expressions as

$$\bar{F}_{rx} = \int_{-1}^{1}\int_{0}^{2\pi}\bar{p}cos\ \alpha d\alpha d\beta \tag{6}$$

$$\bar{F}_{rz} = \int_{-1}^{1}\int_{0}^{2\pi}\bar{p}sin\ \alpha d\alpha d\beta \tag{7}$$

The resultant fluid-film reaction is expressed as

$$\bar{F}_g = \sqrt{\bar{F}_{rx}^2 + \bar{F}_{rz}^2} \tag{8}$$

4.2 Fluid-film stiffness coefficients

The fluid-film stiffness coefficients are defined as (Rajput et al., 2017; Yadav et al., 2017).

$$S_{ij} = \frac{\partial \bar{F}_i}{\partial q_j}(i = x, z) \tag{9}$$

Where " i " represents the direction of force and q_j represents the displacement of journal center coordinate ($\bar{x}_j$ or $\bar{z}_j$).

The stiffness coefficient matrix is given by

(10)

$$S = \begin{bmatrix} \bar{S}_{xx} & \bar{S}_{xz} \\ \bar{S}_{zx} & \bar{S}_{zz} \end{bmatrix} = \begin{bmatrix} \frac{\partial \bar{F}_{rx}}{\partial \bar{x}_J} & \frac{\partial \bar{F}_{rx}}{\partial \bar{z}_J} \\ \frac{\partial \bar{F}_{rz}}{\partial \bar{x}_J} & \frac{\partial \bar{F}_{rz}}{\partial \bar{z}_J} \end{bmatrix}$$

Where,

$$\bar{S}_{xx} = \frac{\partial \bar{F}_{rx}}{\partial \bar{x}_j} = \int_{-1}^{1} \int_{0}^{2\pi} \frac{\partial \bar{p}}{\partial \bar{x}_j} \cos \alpha d\alpha d\beta \quad (11a)$$

$$\bar{S}_{zx} = \frac{\partial \bar{F}_{rz}}{\partial \bar{x}_j} = \int_{-1}^{1} \int_{0}^{2\pi} \frac{\partial \bar{p}}{\partial \bar{x}_j} \sin \alpha d\alpha d\beta \quad (11b)$$

$$\bar{S}_{xz} = \frac{\partial \bar{F}_{rx}}{\partial \bar{z}_j} = \int_{-1}^{1} \int_{0}^{2\pi} \frac{\partial \bar{p}}{\partial \bar{z}_j} \cos \alpha d\alpha d\beta \quad (11c)$$

$$\bar{S}_{zz} = \frac{\partial \bar{F}_{rz}}{\partial \bar{z}_j} = \int_{-1}^{1} \int_{0}^{2\pi} \frac{\partial \bar{p}}{\partial \bar{z}_j} \sin \alpha d\alpha d\beta \quad (11d)$$

4.3 Fluid-film damping coefficients

The fluid-film damping coefficients are defined as (Yadav et al., 2014; Rajput et al., 2017).

$$\bar{C}_{ij} = \frac{\partial \bar{F}_i}{\partial \dot{q}_j} (i = x, z) \quad (12)$$

$\dot{q}_j$ represents the velocity component of journal center ($\dot{\bar{x}}_j$ or $\dot{\bar{z}}_j$).

The damping coefficient matrix is given by:

$$\bar{C} = \begin{bmatrix} \bar{C}_{xx} & \bar{C}_{xz} \\ \bar{C}_{zx} & \bar{C}_{zz} \end{bmatrix} = \begin{bmatrix} \frac{\partial \bar{F}_{rx}}{\partial \dot{\bar{x}}_J} & \frac{\partial \bar{F}_{rx}}{\partial \dot{\bar{z}}_J} \\ \frac{\partial \bar{F}_{rz}}{\partial \dot{\bar{x}}_J} & \frac{\partial \bar{F}_{rz}}{\partial \dot{\bar{z}}_J} \end{bmatrix} \quad (13)$$

$$\bar{C}_{xx} = \frac{\partial \bar{F}_{rx}}{\partial \dot{\bar{x}}_j} = \int_{-1}^{1} \int_{0}^{2\pi} \frac{\partial \bar{p}}{\partial \dot{\bar{x}}_j} \cos \alpha d\alpha d\beta \quad (14a)$$

$$\bar{C}_{zx} = \frac{\partial \bar{F}_{rz}}{\partial \dot{\bar{x}}_j} = \int_{-1}^{1} \int_{0}^{2\pi} \frac{\partial \bar{p}}{\partial \dot{\bar{x}}_j} \sin \alpha d\alpha d\beta \quad (14b)$$

$$\bar{C}_{xz} = \frac{\partial \bar{F}_{rx}}{\partial \dot{\bar{z}}_j} = \int_{-1}^{1} \int_{0}^{2\pi} \frac{\partial \bar{p}}{\partial \dot{\bar{z}}_j} \cos \alpha d\alpha d\beta \quad (14c)$$

$$\bar{C}_{zz} = \frac{\partial \bar{F}_{rz}}{\partial \dot{\bar{z}}_j} = \int_{-1}^{1} \int_{0}^{2\pi} \frac{\partial \bar{p}}{\partial \dot{\bar{z}}_j} \sin \alpha d\alpha d\beta \quad (14d)$$

4.4 Boundary conditions

The boundary conditions for eq. (1) are applied as follows (Wang et al., 2004; Wang, 2007; Yang et al., 2009; Rashidi et al., 2008; Ram, 2016)

1. To avoid cavitation, the Reynolds boundary conditions are used$\left(\bar{p} = \frac{\partial \bar{p}}{\partial \alpha} = 0\right)$.
2. All the nodes lying on the boundary has been assigned atmospheric pressure$(\bar{p} = 0)$.
3. Air flow rate from input to the bearing system must be equal to air flow rate outside the bearing system.

4.5 Stability study from the developed program

The fluid film reaction in two lobe journal bearing is a nonlinear function of journal position and velocity of rotor center. The equation of motion for two lobe Journal Bearing can be written by equation of inertia force and fluid film force to the unbalance rotor forces. The linearized

equation of motion of the Journal Centre in the non-dimensional form is expressed as (Chen and Gunter, 2007; Garg, 2015):

$$[\bar{M}_J]\{\ddot{\bar{x}}_j\} + [\bar{C}]\{\dot{\bar{x}}_J\} + [S]\{\bar{X}_J\} = [\bar{F}_R] \tag{12}$$

The above equation of motion can be written in matrix form as

$$\begin{bmatrix} \overline{m_J} & 0 \\ 0 & \bar{m}_J \end{bmatrix} \begin{Bmatrix} \ddot{\bar{x}}_j \\ \ddot{\bar{z}}_j \end{Bmatrix} + \begin{bmatrix} \bar{C}_{xx} & \bar{C}_{xz} \\ \bar{C}_{zx} & \bar{C}_{zz} \end{bmatrix} \begin{Bmatrix} \dot{\bar{x}}_j \\ \dot{\bar{z}}_j \end{Bmatrix} + \begin{bmatrix} \bar{S}_{xx} & \bar{S}_{xz} \\ \bar{S}_{zx} & \bar{S}_{zz} \end{bmatrix} \begin{Bmatrix} \bar{x}_j \\ \bar{z}_j \end{Bmatrix} = \begin{Bmatrix} \bar{m}_r \bar{\rho} \bar{\omega}^2 \sin(\tau) \\ \bar{m}_r \bar{\rho} \bar{\omega}^2 \cos(\tau) \end{Bmatrix} \tag{13}$$

The above governing equation of motion has been solved by using the 4th order Runge-Kutta method (Butcher, 1987).

The space state vector for equation of motion can be written as

$$[\mathbf{X}] = \begin{bmatrix} \bar{x}_j \\ \bar{z}_j \\ \dot{\bar{x}}_j \\ \dot{\bar{z}}_j \end{bmatrix} \quad , \quad [\mathbf{X}] = \begin{bmatrix} X_J \\ Z_J \\ \dot{X}_J \\ \dot{Z}_J \end{bmatrix} \quad , \quad [\dot{\mathbf{X}}] = \begin{bmatrix} \dot{X}_J \\ \dot{Z}_J \\ \ddot{X}_J \\ \ddot{Z}_J \end{bmatrix} \tag{14}$$

These are computed as

$$\mathbf{X} = \mathrm{f}(\mathbf{X}) \tag{15a}$$
$$\mathbf{k}_1 = \mathrm{f}(\mathbf{X}_i) \tag{15b}$$
$$\mathbf{k}_2 = \mathrm{f}\left(\mathbf{X}_i + \mathbf{k}_1 \times \frac{\Delta t}{2}\right) \tag{15c}$$
$$\mathbf{k}_3 = \mathrm{f}\left(\mathbf{X}_i + \mathbf{k}_2 \times \frac{\Delta t}{2}\right) \tag{15d}$$
$$\mathbf{k}_4 = \mathrm{f}(\mathbf{X}_i + \mathbf{k}_3 \times \Delta t) \tag{15e}$$

After computing coefficients $\mathbf{k}_1$, $\mathbf{k}_2$, $\mathbf{k}_3$ and $\mathbf{k}_4$ the updated positions and journal centre velocities are calculated as

$$\mathbf{X}_{i+1} = \mathbf{X}_i + \left(\frac{\mathbf{k}_1 + 2\mathbf{k}_2 + 2\mathbf{k}_3 + \mathbf{k}_4}{6}\right) \times \Delta t \tag{16}$$

The X_i is used to plot trajectory and bifurcation plots from the solution. The chosen value of Δt is $2\pi/N$ and N is 200.

4.6 Convergence criteria

The following convergence criteria has been used to compute equilibrium position of the journal centre.

$$\frac{\left(\left((\bar{x}_j)_{i+1} - (\bar{x}_j)_i\right)^2 + \left((\bar{z}_j)_{i+1} - (\bar{z}_j)_i\right)^2\right)}{(\bar{x}_j)_{i+1}^2 + (\bar{z}_j)_{i+1}^2} < 0.0001 \tag{17}$$

5.0 RESULTS AND DISCUSSION

To validate the develop finite element formulation the results of study has been compared with the already published study, as shown. It is found that the results of the developed program are in good agreement with the results in available literature (Table 1). Maximum percentage error in the comparison is 1.05 %. In the present simulation, non-dimensional parameters are used to produce results by using bearing parameter defined in Table 2:

Table 1: Validation of results as compared with Yang et al., 2009.

	$\overline{F}_g$	$\bar{e}_0$(Present results by FEM)	$\bar{e}_0$(Yang, et al., 2009 by FDM)	Percentage difference
U=0.1	0.0892	0.1003	0.1	0.3 %
	0.1828	0.2007	0.2	0.35 %
	0.404	0.4006	0.4	0.15 %
	0.752	0.6006	0.6	0.10 %
	1.712	0.8013	0.8	0.16 %
U=0.5	0.3448	0.1010	0.1	1.00 %
	0.704	0.2021	0.2	1.05 %
	1.544	0.4032	0.4	0.80 %
	2.88	0.6020	0.6	0.33 %
	6.22	0.8015	0.8	0.19 %

Table 2: Geometric and operating parameters used for gas bearing.

S. No.	Bearing parameters	Value
1	Bearing diameter (D)	50 mm
2	Bearing length (L)	50 mm
3	Radius clearance (c)	10 μm
4	Ellipticity ratio (δ)	0.7-1.3
5	Atmospheric pressure (p_a)	1.01325×10^5 Pa
6	Air viscosity (η)	1.79756×10^{-5} N·s/m^2
7	Air density (ρ)	1.204 Kg/m^3
8	Air temperature (T)	293 K
9	Acceleration of gravity (g)	9.8 m/s^2
10	Isentropic expansion index of gas (κ)	1.4
11	Air/Gas constant (R_g)	29.253 N·s^2/(Kg·K)
12	Rotation velocity of journal	12000 rpm
13	Eccentricity ratio ($\bar{e}$)	0 to .6

The simulation time to generate bifurcation diagram for the gas bearing is about 24 hours. The time step size is $\frac{\pi}{120}$. The time series data of the first 20000-time steps are excluded from dynamic behavior investigation. To solve Reynold equation, air film is discretized by using the four Noded isoparametric quadrilateral elements. Elemental finite element matrix is generated and assembled into global fluidity matrix. Figure 3 shows the bifurcation diagram of two lobe and circular gas journal bearing. As shown in figure 3, the two-lobe gas journal bearing $\bar{\omega} > 1.8$ and $\delta = 0.7$ becomes unstable. While circular bearing with $\bar{\omega} > 1.4$ and $\delta = 1$ becomes unstable. Hence two lobe aerodynamic bearing $\delta = 0.7$ is more stable as comparison to other bearings.

Bifurcation map is widely used to analyze the behavior of dynamic system. Bifurcation map in Figure 4 has been plotted for two lobe aerodynamic bearing by taking journal mass as a system variable. In this the two-lobe bearing with offset factor ($\delta = 1.3$). For the value of $\bar{m}_r > 40$, the bearing offset factor ($\delta = 0.7$) and 1 bearing become unstable whereas the bearing offset factor $\delta = 1.3$ bearing become stable at for the value of $\bar{m}_r > 50$. Therefore, two-lobe bearing with offset factor ($\delta = 1.3$) is more stable.

Poincaré map is widely used to analyze the behavior of dynamic system. Figure 5 represents Poincaré map of two-lobe bearing for the different value of offset ration and journal mass. As the mass and speed increases the bearing becomes unstable because of unbalanced forces on the bearing. The bearing for the values of $\delta = 0.7, \bar{m}_r = 20$, and $\bar{\omega} = 2.1$ shows the chaotic motion for two-lobe bearing. The bearing having values $\delta = 1.3$, $\bar{m}_r = 20$, and $\bar{\omega} = 1.8$ shows a stable Poincaré map. The bearing having values $\delta = 1, \bar{m}_r = 20$, and $\bar{\omega} = 2.1$ shows the complete unstable Poincaré map.

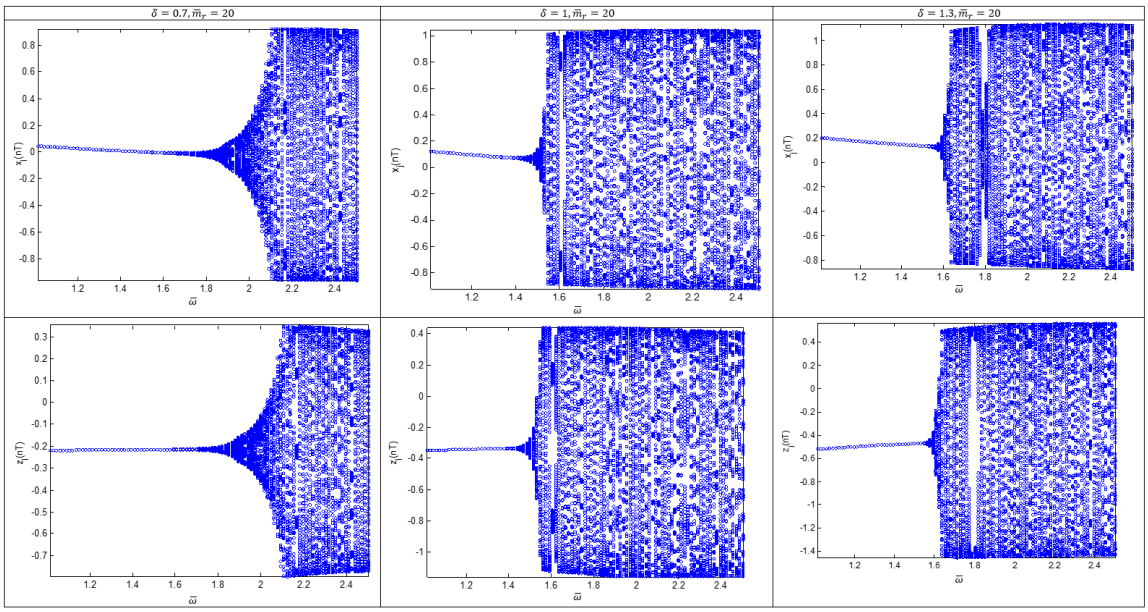

Figure 3: Bifurcation diagram of two lobe aerodynamic journal bearing with different offset factor.

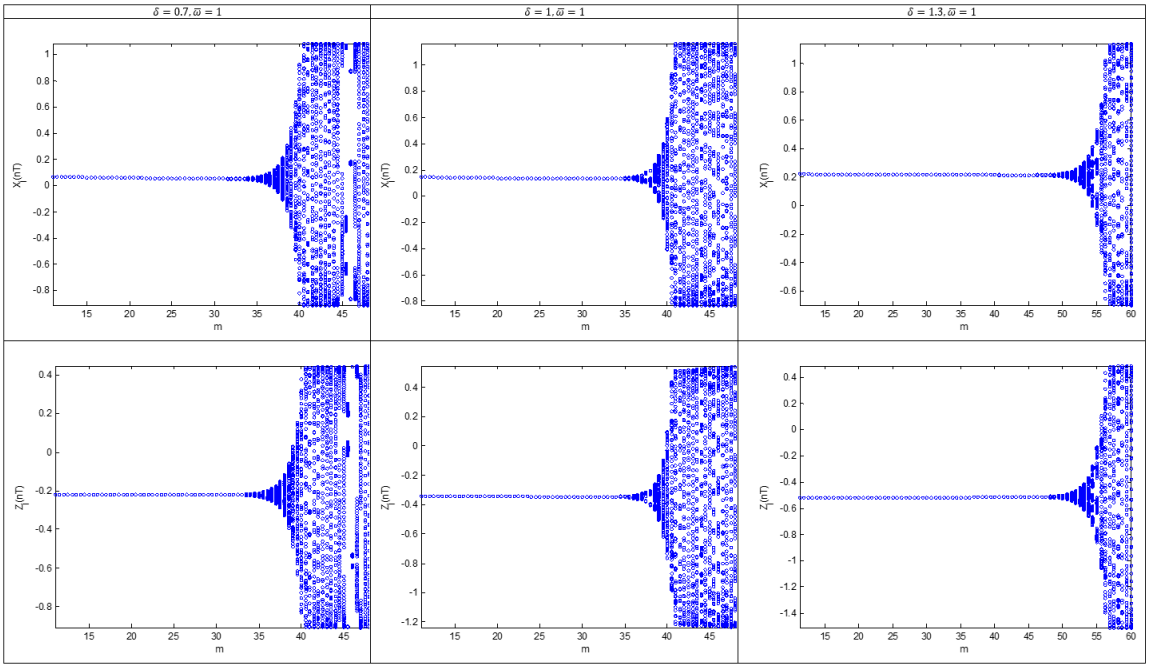

Figure 4: Bifurcation diagram by taking rotor mas as system parameter with different offset factor.

6.0 CONCLUSIONS

In the present work, dynamic analysis of two lobe bearing has been done and dynamic performance of bearing has been compared. The results are presented in the form of Bifurcation and Poincaré map. Bifurcation and Poincaré map is an effective method to present system behavior. Based on above results and discussion following foremost conclusion has been drawn.

1. The two-lobe journal bearing is more stable in comparison to circular journal bearing.
2. Stability and dynamic response of bearing is greatly affected by the offset ratio of the bearing.
3. The variation of ellipticity ratio of the two lobe bearing plays a major role in the dynamics of bearing.
4. The results developed in this study will help bearing designer to avoid undesirable behavior of rotor center trajectory and bearing center trajectory, hence life of rotor system will increase.

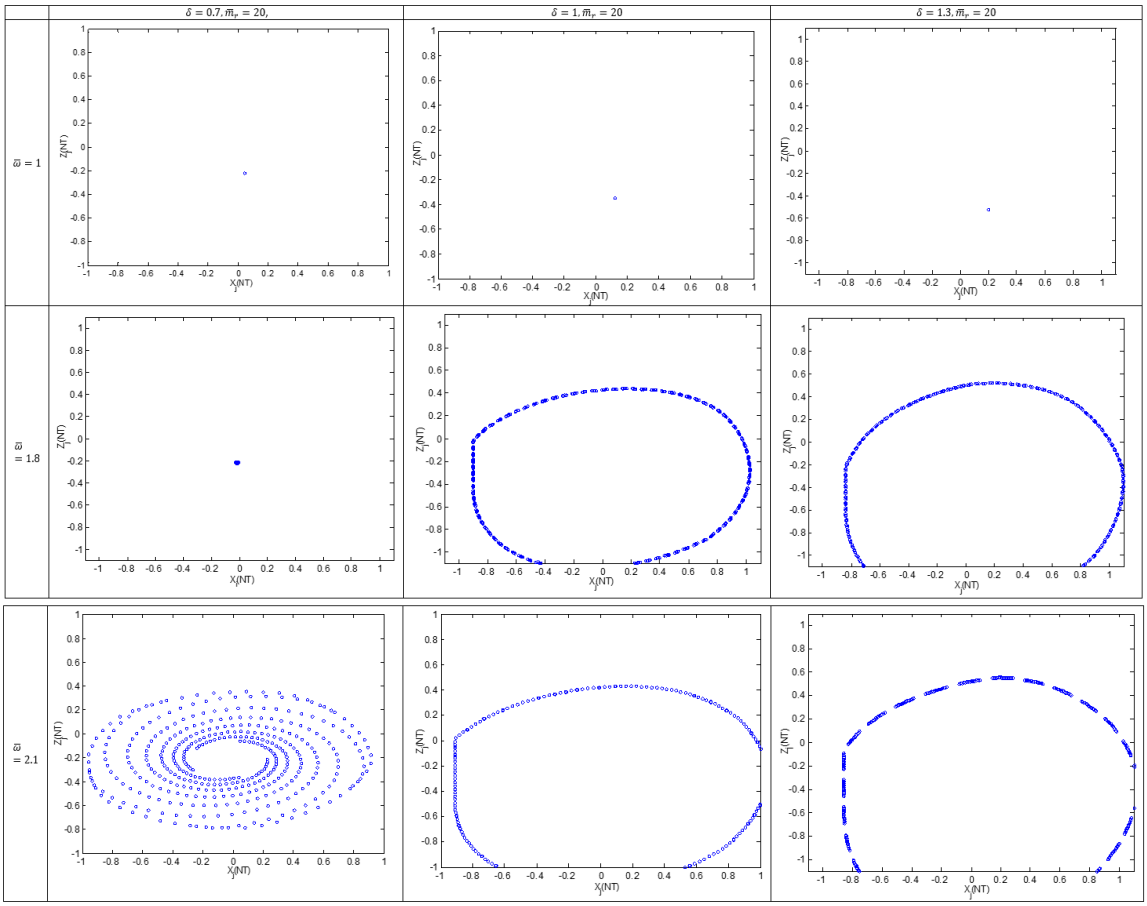

Figure 5: Poincare map of two lobe aerodynamic journal bearing with different offset factor and velocity.

REFERENCES

Awasthi, R. K., Jain, S. C., & Sharma, S. C. (2006). Finite element analysis of orifice-compensated multiple hole-entry worn hybrid journal bearing. Finite Elements in Analysis And Design, 42(14-15), 1291-1303.

Butcher, J. C. (1987). The numerical analysis of ordinary differential equations: Runge-Kutta and general linear methods.

Chen, C. L., & Yau, H. T. (1998). Chaos in the imbalance response of a flexible rotor supported by oil film bearings with non-linear suspension. Nonlinear Dynamics, 16(1), 71-90.

Chen, W. J., & Gunter, E. J. (2007). Introduction to dynamics of rotor-bearing system. Trafford, Victoria. BC, Canada.

Dhatt, G., E. Lefrançois and G. Touzot (2012). Finite element method, John Wiley & Sons.

Elrod, H. G., McCabe, J. T., & Chu, T. Y. (1967). Determination of gas-bearing stability by response to a step-jump. Journal of Lubrication Technology, 89(4), 493-498.

Garg, H. C. (2015). Stability analysis of slot-entry hybrid journal bearings operating with non-newtonian lubricant. Jurnal Tribologi, 6, 1-23.

Holster, P. L., & Jacobs, J. A. H. (1987). Theoretical analysis and experimental verification on the static properties of externally pressurized air-bearing pads with load compensation. Tribology international, 20(5), 276-289.

Kushare, P. B., & Sharma, S. C. (2014). Nonlinear transient stability study of two lobe symmetric hole entry worn hybrid journal bearing operating with non-Newtonian lubricant. Tribology International, 69, 84-101.

Lihua, Y., Huiguang, L., & Lie, Y. (2007). Dynamic stiffness and damping coefficients of aerodynamic tilting-pad journal bearings. Tribology International, 40(9), 1399-1410.

Ma, W., Cui, J., Liu, Y., & Tan, J. (2016). Improving the pneumatic hammer stability of aerostatic thrust bearing with recess using damping orifices. Tribology International, 103, 281-288.

Malik, M., & Bert, C. W. (1994). Differential quadrature solutions for steady-state incompressible and compressible lubrication problems. Journal of Tribology, 116(2), 296-302.

Piekos, E. S. (2000). Numerical simulation of gas-lubricated journal bearings for microfabricated machines (Doctoral dissertation, Massachusetts Institute of Technology).

Rajput, A. K., Yadav, S. K., & Sharma, S. C. (2017). Effect of geometrical irregularities on the performance of a misaligned hybrid journal bearing compensated with membrane restrictor. Tribology International, 115, 619-627.

Ram, N. (2016). Numerical analysis of capillary compensated micropolar fluid lubricated hole-entry journal bearings. Jurnal Tribologi, 9, 18-44.

Rashidi, R., Karami, M. A., & Bakhtiari, N. F. (2008). Preload effect on nonlinear dynamic behavior of aerodynamic two-lobe journal bearings. Journal of Aerospace Science and Technology (JAST), 5(4), 145-159.

Sharma, S. C., Jain, S. C., & Bharuka, D. K. (2002). Influence of recess shape on the performance of a capillary compensated circular thrust pad hydrostatic bearing. Tribology International, 35(6), 347-356.

Sinhasan, R., & Sah, P. L. (1996). Static and dynamic performance characteristics of an orifice compensated hydrostatic journal bearing with non-Newtonian lubricants. Tribology International, 29(6), 515-526.

Wang, C. C. (2007). Bifurcation analysis of an aerodynamic journal bearing system considering the effect of stationary herringbone grooves. Chaos, Solitons & Fractals, 33(5), 1532-1545.

Wang, C. C., Jang, M. J., & Chen, C. O. K. (2004). Non-linear dynamic analysis of a flexible rotor supported by self-acting gas journal bearings. Proceedings of the Institution of Mechanical Engineers, Part C: Journal of Mechanical Engineering Science, 218(12), 1527-1538.

Yabe, H., & Ikuno, Y. (1996). A study on sliding accuracy characteristics of an externally pressurized gas-lubricated guide way: Fundamental sliding accuracy characteristics. JSME International Journal. Ser. C, Dynamics, Control, Robotics, Design and Manufacturing, 39(2), 371-377.

Yadav, S. K., & Sharma, S. C. (2014). Performance of hydrostatic tilted thrust pad bearings of various recess shapes operating with non-Newtonian lubricant. Finite Elements in Analysis and Design, 87, 43-55.

Yadav, S. K., Rajput, A. K., Ram, N., & Sharma, S. C. (2017). A direct numerical approach to compute the nonlinear rotor dynamic coefficient of the noncircular gas journal bearing. Proceedings of the Institution of Mechanical Engineers, Part J: Journal of Engineering Tribology, In Press. https://doi.org/10.1177/1350650117719602.

Yang, L. H., Wang, W. M., Zhao, S. Q., Sun, Y. H., & Yu, L. (2014). A new nonlinear dynamic analysis method of rotor system supported by oil-film journal bearings. Applied Mathematical Modelling, 38(21-22), 5239-5255.

Yang, P., Zhu, K. Q., & Wang, X. L. (2009). On the non-linear stability of self-acting gas journal bearings. Tribology International, 42(1), 71-76.